ISSN 0036-0236, Russian Journal of Inorganic Chemistry, 2020, Vol. 65, No. 11, pp. 1687–1694. © Pleiades Publishing, Ltd., 2020.
Russian Text © The Author(s), 2020, published in Zhurnal Neorganicheskoi Khimii, 2020, Vol. 65, No. 11, pp. 1497–1505.

COORDINATION COMPOUNDS

High-Temperature Spin Crossover in Complexes of Iron(II) *closo*-Borates with 2,6-Bis(benzimidazol-2-yl)pyridine

A. D. Ivanova[a], L. G. Lavrenova[a, b, *], E. V. Korotaev[a], S. V. Trubina[a], L. A. Sheludyakova[a], S. A. Petrov[c], K. Yu. Zhizhin[d], and N. T. Kuznetsov[d]

[a] *Nikolaev Institute of Inorganic Chemistry, Siberian Branch, Russian Academy of Sciences, Novosibirsk, 630090 Russia*
[b] *Novosibirsk National Research State University, Novosibirsk, 630090 Russia*
[c] *Institute of Solid State Chemistry, Siberian Branch, Russian Academy of Sciences, Novosibirsk, 630128 Russia*
[d] *Kurnakov Institute of General and Inorganic Chemistry, Russian Academy of Sciences, Moscow, 119991 Russia*
**e-mail: ludm@niic.nsc.ru*

Received June 17, 2020; revised June 24, 2020; accepted June 26, 2020

Abstract—New iron(II) complexes with 2,6-bis(benzimidazol-2-yl)pyridine (L) and *closo*-borate(2–) anions—$[FeL_2][B_{10}H_{10}] \cdot 2H_2O$ and $[FeL_2][B_{12}H_{12}] \cdot H_2O$—have been synthesized. The complexes have been characterized by static magnetic susceptibility measurements, electronic (diffuse reflectance spectra), IR, and EXAFS spectroscopy, and X-ray diffraction analysis. A study of the $\mu_{eff}(T)$ dependence in the temperature range 80–500 K has shown that the complexes exhibit a high-temperature spin crossover $^1A_1 \Leftrightarrow {}^5T_2$.

Keywords: synthesis, complexes, iron(II), 2,6-bis(benzimidazol-2-yl)pyridine, cluster boron anions, electronic, IR, and EXAFS spectroscopy, XRD, spin crossover

DOI: 10.1134/S0036023620110078

Spin crossover (SCO, spin transition) can manifest itself in $3d^4$–$3d^7$ metal complexes with an octahedral or pseudo-octahedral environment of ligands of a certain field strength. The change in the spin multiplicity occurs in response to external stimuli: change in temperature and pressure, irradiation with light of a certain wavelength, and other factors. Monographs and numerous reviews and articles [1–9] have been devoted to the study of this phenomenon. Compounds capable of existing in two states with a sufficiently long lifetime are promising for use as active elements in electronic devices [3, 10–15]. One of the classes of compounds in which a spin crossover is observed includes octahedral iron(II) complexes with polynitrogen-containing heterocyclic ligands forming the FeN_6 coordination core. In a number of such compounds, thermally induced SCO is observed. The temperature and nature of the spin transition in these complexes depend on a number of factors, in particular, on their structure, the nature of the ligand and anion, the presence and number of crystallization solvent molecules, e.g., water, in the structure. It should be especially noted that the SCO temperature significantly depends on the anions occupying the outer-sphere position in these complexes.

In the present work, 2,6-bis(benzimidazol-2-yl)pyridine (L) (Scheme 1) has been used as a ligand for the synthesis of complexes. Before the beginning of our work, only a few iron(II) compounds with L were known to possess SCO, in particular, Fe(II) perchlorate and tetraphenylborate complexes of [16, 17]. We have synthesized a number of Fe(II) complexes with L of the composition $[FeL_2]A_i \cdot nH_2O$ ($A = SO_4^{2-}$, SiF_6^{2-}, ReO_4^-; Br^-, NO_3^-, $C_2N_3^-$; $i = 1, 2$; $n = 0.5$–2) in which the SCO is observed [18, 19]. In continuation of these works, we have synthesized and studied iron(II) complexes with L, containing cluster boron anions $[B_{10}H_{10}]^{2-}$ and $[B_{12}H_{12}]^{2-}$. The salts of boron cluster anions are promising for the synthesis of biologically active complexes, including cytotoxic drugs [20–24].

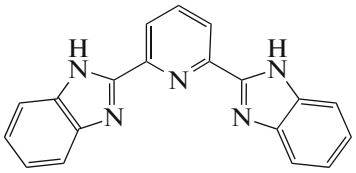

Scheme 1. Structure of 2,6-bis(benzimidazol-2-yl)pyridine (L).

Previously, we synthesized iron(II) complexes with polynitrogen-containing ligands, in particular, with 1,2,4-triazoles and tris(pyrazol-1-yl)methanes, containing $[B_{10}H_{10}]^{2-}$ and $[B_{12}H_{12}]^{2-}$ as outer-sphere anions [8, 25–27]. Most of these compounds show spin crossover. It seemed expedient to continue research along this line. The search for new bi- and polyfunctional compounds is an important scientific challenge.

EXPERIMENTAL

For the synthesis, $FeSO_4 \cdot 7H_2O$ (Acros Organics), ascorbic acid medicinal, 2,6-bis(benzimidazol-2-yl)pyridine (Aldrich), and ethanol rectified were used. All reagents were used as purchased. The $K_2[B_{10}H_{10}] \cdot 2H_2O$ and $K_2[B_{12}H_{12}]$ complexes were synthesized as described elsewhere [28].

Synthesis of $[FeL_2][B_{10}H_{10}] \cdot 2H_2O$ (1) and $[FeL_2][B_{12}H_{12}] \cdot H_2O$ (2). A 0.14-g (0.5 mmol) sample of $FeSO_4 \cdot 7H_2O$ was dissolved in 6 mL of distilled water acidified with 0.12 g of ascorbic acid. To this solution, a 1.5-fold excess of $K_2[B_{10}H_{10}] \cdot 2H_2O$ (0.17 g, 0.75 mmol) or $K_2[B_{12}H_{12}]$ (0.17 g, 0.75 mmol) in 5 mL of water was added under stirring. Then, to each of the resulting solutions, a warm solution of 0.31 g (1 mmol) of L in 25 mL of ethanol was slowly added. Dark violet precipitates appeared immediately after mixing the solutions, which were stirred by a magnetic stirrer for 5 h. The precipitates were filtered off, washed two times with 1 mL of water and 1 mL of ethanol, and dried in air. The yield of compounds **1** and **2** was 95 and 85%, respectively.

For $C_{38}H_{40}B_{10}FeN_{10}O_2$ (**1**) anal. calcd. (%): C, 54.8; H, 4.8; N, 16.8.

Found (%): C, 54.5; H, 4.4; N, 16.6.

For $C_{38}H_{40}B_{12}FeN_{10}O$ (**2**) anal. calcd. (%): C, 54.4; H, 4.8; N, 16.7.

Found (%): C, 54.2; H, 5.0; N, 16.3.

C, H, N elemental analysis was carried out on a EuroVector EURO EA 3000 analyzer in the analytical laboratory of the Institute of Inorganic Chemistry, SB RAS.

X-ray diffraction analysis of fine crystalline compounds was performed on a Shimadzu XRD 7000 diffractometer (CuK_α radiation, Ni filter, scintillation detector) at room temperature.

Static magnetic susceptibility of the samples was measured by the Faraday method in the temperature range 80–480 K. Temperature stabilization of the sample with an accuracy of 1 K during measurements was carried out using a Delta Electronics DTB9696 temperature controller. The heating and cooling rates of the samples were ~2–3 K/min. The external magnetic field strength of 7.3 kOe during the studies was maintained with a stabilization accuracy of ~2%. To study the dehydrated complexes, the samples under study were placed in open quartz ampoules and evacuated to a residual pressure in the measuring cell of 10^{-2} mm Hg, then an inert helium atmosphere at a pressure of 5 mm Hg was created. In the study of compounds containing crystallization water, the samples were sealed with atmospheric air in quartz ampoules. The effective magnetic moment was calculated by the formula $\mu_{eff} = \left(8\chi'_M T\right)^{1/2}$, where χ'_M is the molar magnetic susceptibility corrected for the diamagnetic contribution according to the Pascal scheme. The temperatures of the direct ($T_c\uparrow$) and reverse ($T_c\downarrow$) transitions of the complexes under study were determined based on the condition $d^2\mu_{eff}/dT^2 = 0$.

IR absorption spectra were recorded on Scimitar FTS 2000 (4000–400 cm^{-1}) and Vertex 80 (400–100 cm^{-1}) IR FT spectrophotometers. Samples were prepared as mineral and fluorinated oil mulls and polyethylene pellets.

Kubelka–Munk diffuse reflectance spectra (DRS) were recorded on a Shimadzu UV-3101 PC scanning spectrophotometer at room temperature.

Mössbauer spectra of the complexes were measured at 295 K on an NP-610 spectrometer with a ^{57}Co (Rh) source.

Fe*K* edge X-ray absorption spectra were collected in the standard transmission mode in the range 800 eV above the absorption edge (7112 eV) using a Si(111) double-crystal monochromator. The studies were performed on beamline 8 of the VEPP-3 storage ring, Siberian Synchrotron and Terahertz Radiation Center, Institute of Nuclear Physics, SB RAS. Measurements for $[FeL_2][B_{10}H_{10}] \cdot 2H_2O$ were carried out at two temperatures: $T \sim 300$ K (the compound in the low-spin (LS) state) and $T = 450$ K (the compound in the high-spin (HS) state). For $[FeL_2][B_{12}H_{12}] \cdot H_2O$, the measurement was performed only at room temperature. When heated, the sample was placed in an furnace open at both ends; the temperature was controlled with a chromel–alumel thermocouple. The oscillating part ($\chi(k)$) of the absorption spectrum was obtained with the VIPER software; the simulation was carried out with the EXCURV program for unfiltered (raw) spectra in the approximation of multiple scattering of the whole molecule without considering cluster boron anions. In modeling the structure of the ligand (L), in order to reduce the number of variable parameters, benzene rings were not taken into account, which, due to their structural distance from the central iron atom, have a weak effect on the shape of the EXAFS spectrum. The modeling procedure was carried out in the range of wave vectors $\Delta k = 3.0–13$ $Å^{-1}$ with the weighting coefficient $w = k^3$ and the amplitude suppression factor $S_0^2 = 1.0$.

RESULTS AND DISCUSSION

The $[FeL_2][B_{10}H_{10}] \cdot 2H_2O$ and $[FeL_2][B_{12}H_{12}] \cdot H_2O$ complexes were isolated from a water/ethanol system at a Fe^{2+} concentration of ~0.15 mol/L and the stoichiometric Fe : L ratio. Ascorbic acid was used as a reducing agent and a weakly acidifying reagent. At the first stage, a solution of iron(II) *closo*-borate was prepared from an aqueous solution of $FeSO_4$ with the use of a 1.5-fold excess of the $K_2[B_{10}H_{10}] \cdot 2H_2O$ or $K_2[B_{12}H_{12}]$ salt. At the second stage, these solutions were reacted with an ethanol solution of the ligand. The complexes were isolated in high yield (80–90%).

Table 1. Selected vibrational frequencies (cm^{-1}) in the spectra of L and complexes **1** and **2**

Compound			Assignment
L	**1**	**2**	
	3460	3630 3594 3513	ν(O–H)
3173 3150	3210 3183	3274	ν(N–H)
3070	3077 3054	3077 3048	ν(C–H)
	2463 2435	2485 2405	ν(B–H)
1601 1589 1574 1541 1489	1609 1591 1528 1486	1610 1591 1530 1488	R_{ring}
–	280	280	ν(M–N)

Table 1 presents key vibrational bands of L and complexes **1** and **2**. The high-frequency range of the spectra of the complexes (3460–3630 cm^{-1}) shows O–H stretching vibration bands. The spectrum of L shows in the range 3400–2800 cm^{-1} broad stretching vibration bands of NH groups involved in hydrogen bonds. In the spectra of the complexes, the ν(NH) bands become narrower and are observed at 3210 and 3183 cm^{-1} (**1**) and 3274 cm^{-1} (**2**). The high-frequency shift of the ν(NH) bands and their clearer manifestation in comparison with the L spectrum is probably associated with the weakening of hydrogen bonds on going from the ligand to the complexes. In the range 2500–2400 cm^{-1}, the spectra show B–H stretching vibration bands. The position of the bands in the range of ring vibrations in the spectra of complexes **1** and **2** noticeably changes in comparison with that in the spectrum of L, which indicates the coordination of the nitrogen atoms of heterocycles to iron(II). This is also supported by the character of the spectra of **1** and **2** in the low-frequency range. There are bands at 280 cm^{-1} that are absent in the spectrum of the ligand, which can be attributed to the M–N stretching vibrations.

The DRS of complexes **1** and **2** in the visible and near-IR ranges show two broad absorption bands at 537 and 755 nm (**1**) and 510 and 709 nm (**2**). The bands in the 500–540 nm range with maxima at 537 (**1**) and 510 (**2**) cm^{-1} can be assigned to the *d–d* transition $^1A_1 \rightarrow {}^1T_1$ in a strong distorted octahedral ligand field. The position of these bands is typical of low-spin octahedral iron(II) complexes with nitrogen-containing ligands with the FeN_6 chromophore [4, 26]. The absorption bands in the range of 700–760 nm with maxima at 755 (**1**) and 709 nm (**2**) refer to the *d–d* transition $^5T_2 \rightarrow {}^5E$ in high-spin octahedral Fe(II) complexes with nitrogen-containing ligands. For these forms of complexes, $\nu_{HS} = \Delta_{HS}$. The splitting parameters for **1** and **2** have been calculated using the following approximations: $\nu_{LS} = \Delta_{LS} - C + 86B^2/\Delta_{LS}$, $\Delta_{HS} \approx 19B$, and $C = 4.41B$ [29–31] (Table 2). Comparison of the splitting parameters for the three classes of compounds studied by us—Fe(II) complexes with 1,2,4-triazoles [4], tris(pyrazol-1-yl)methanes [4], and 2,6-bis(benzimidazol-2-yl)pyridine ([19] and this work)—shows that the latter produces a stronger ligand field as compared to 1,2,4-triazoles, while the splitting parameters Δ_{LS} and Δ_{HS} for the complexes with tris(pyrazol-1-yl)methanes and 2,6-bis(benzimidazol-2-yl)pyridine are close to each other.

The Mössbauer spectra of the complexes (Fig. 1) are a superposition of lines arising from the HS and LS states of iron(II) atoms. The chemical shift δ (with respect to α-Fe) and the quadrupole splitting ε for each of the species have been extracted by processing the experimental spectra (Table 3). In both cases, the major species is the LS form with lower δ and ε values; the α_{HS} value for the complex with the $[B_{12}H_{12}]^{2-}$ anion is almost twice as large as that for the complex with the $[B_{10}H_{10}]^{2-}$ anion.

The difference between the Mössbauer spectra of the iron(II) compounds synthesized in this work with the $[B_{10}H_{10}]^{2-}$ and $[B_{12}H_{12}]^{2-}$ anions from the previously studied complexes of the composition $[FeL_2]A_i$ ($A = SO_4^{2-}$, SiF_6^{2-}, ReO_4^-; Br^-; NO_3^-; $C_2N_3^-$; $i = 1, 2$) [18, 19] is in the presence of lines of the HS iron(II) forms in the spectra at 295 K. The spectra of the previously studied complexes show the lines of the HS iron(II) species at room temperature only in one case. The δ and ε values for the LS forms of complexes **1** and **2** are in the same range of values as for the previously studied compounds. However, the trend in the behavior of these parameters (an increase in ε with an increase in δ), which we revealed earlier, is not observed for complexes with cluster boron anions.

Table 2. Calculated *B* and *C* values and splitting parameters Δ_{HS} and Δ_{LS} of complexes **1** and **2**

Complex	$\nu(^1A_1 \rightarrow {}^1T_1)$, cm^{-1}	$\nu(^5T_2 \rightarrow {}^5E) = \Delta_{HS}$, cm^{-1}	*B*, cm^{-1}	*C*, cm^{-1}	Δ_{LS}, cm^{-1}
1	1.86×10^4	1.32×10^4	697	3.07×10^3	1.96×10^4
2	1.96×10^4	1.41×10^4	742	3.27×10^3	2.06×10^4

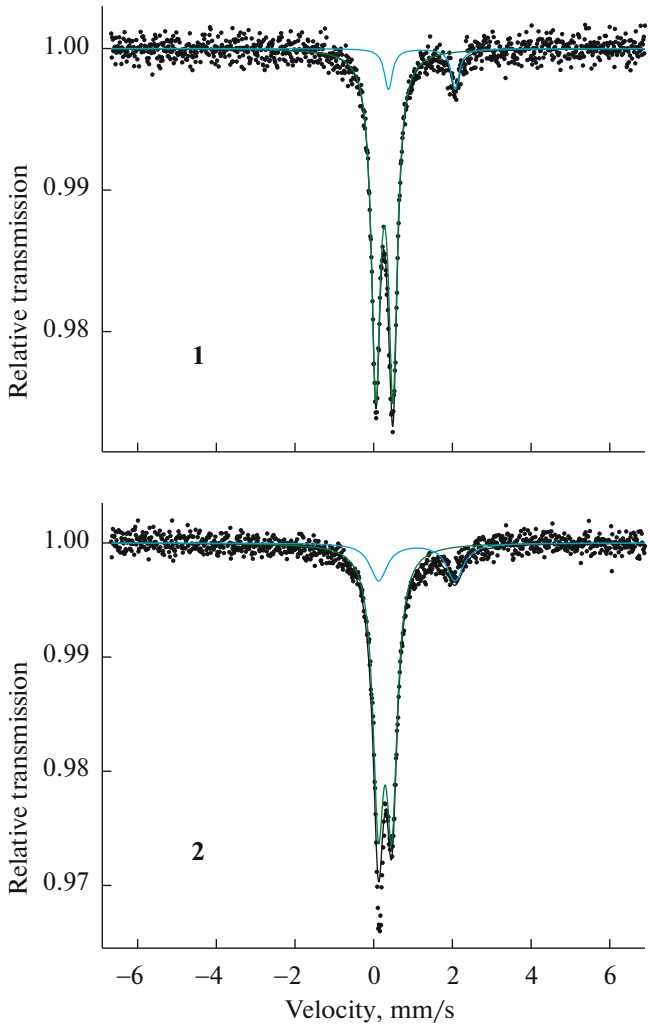

Fig. 1. Mössbauer spectra of complexes **1** and **2**.

Noteworthy is one more feature of the Mössbauer spectra of complexes **1** and **2**: the lines of the quadrupole doublet for the HS form of the complex with the $[B_{10}H_{10}]^{2-}$ anion are narrow, and those for the complex with the $[B_{12}H_{12}]^{2-}$ anion are broader. This suggests that the HS form generated upon spin crossover is well crystallized in the first case and is weakly crystallized state in the second case.

Figure 2 shows the Fe*K* XANES spectra of $[FeL_2][B_{10}H_{10}] \cdot 2H_2O$ (solid line) and $[FeL_2][B_{12}H_{12}] \cdot H_2O$ (circles) measured at 300 K and $[FeL_2][B_{12}H_{12}] \cdot H_2O$ (dashed line) measured at 450 K. For the sample measured at $T = 450$ K and being in the high-spin state (dashed line), the absorption edge is displaced toward higher energies, which is evidence of an increase in the positive charge at the iron atom. Figures 3 and 4 show

Table 3. Parameters of the Mössbauer spectra of complexes **1** and **2**

Complex	δ, mm/s	ε, mm/s	$\Gamma_{1,2}$, mm/s	α_{HS}
$[FeL_2][B_{10}H_{10}] \cdot 2H_2O$ (**1**)	0.272 (LS)	0.435	0.266	10.4
	1.223 (HS)	1.698	0.245	
$[FeL_2][B_{12}H_{12}] \cdot H_2O$ (**2**)	0.289 (LS)	0.344	0.350	19.2
	1.094 (HS)	1.939	0.531	
Error	±0.001	±0.002	±0.010	

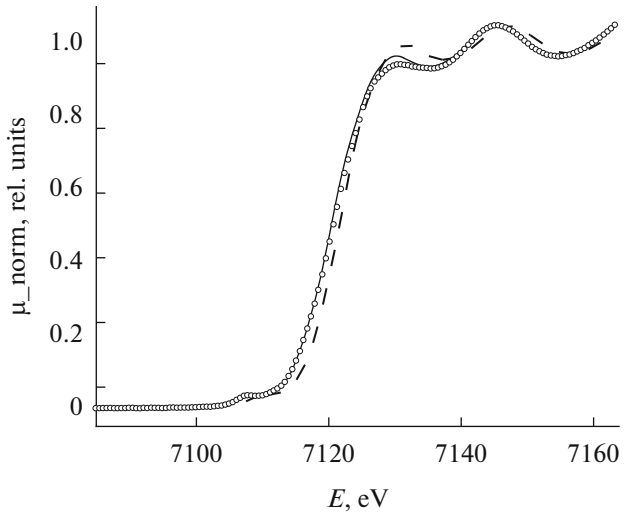

Fig. 2. Fe*K* XANES spectra of (solid line) $[FeL_2][B_{10}H_{10}] \cdot 2H_2O$ and (circles) $[FeL_2][B_{12}H_{12}] \cdot H_2O$ measured at 300 K and of (dashed line) $[FeL_2][B_{12}H_{12}] \cdot H_2O$ measured at 450 K.

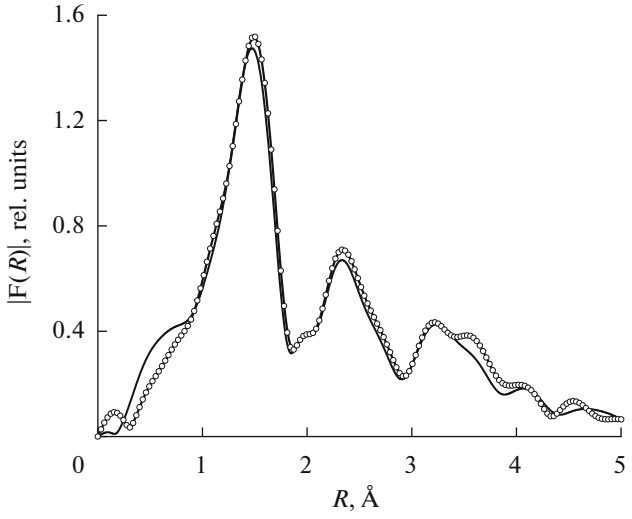

Fig. 3. Fourier transform magnitudes of experimental Fe*K* EXAFS spectra ($k^2\chi(k)$) not corrected for phase shift of the (solid line) $[FeL_2][B_{10}H_{10}] \cdot 2H_2O$ and (circle) $[FeL_2][B_{12}H_{12}] \cdot H_2O$ complexes. Measurements were performed at room temperature.

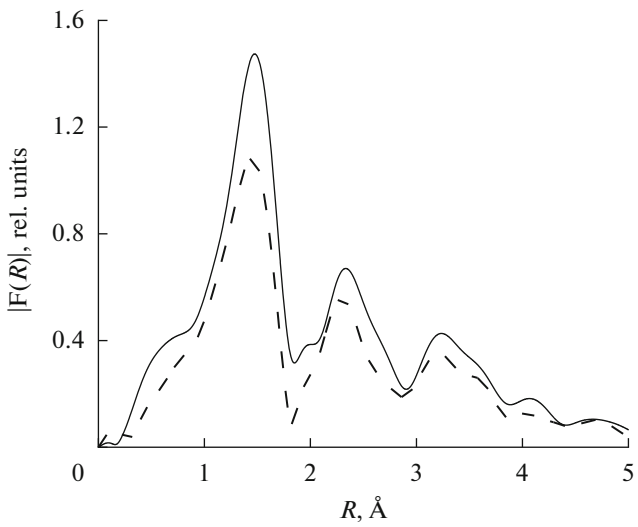

Fig. 4. Fourier transform magnitudes of experimental Fe*K* EXAFS spectra ($k^2\chi(k)$) not corrected for phase shift of the $[FeL_2][B_{12}H_{12}] \cdot H_2O$ complex measured (solid line) at room temperature and (dashed line) at $T = 450$ K.

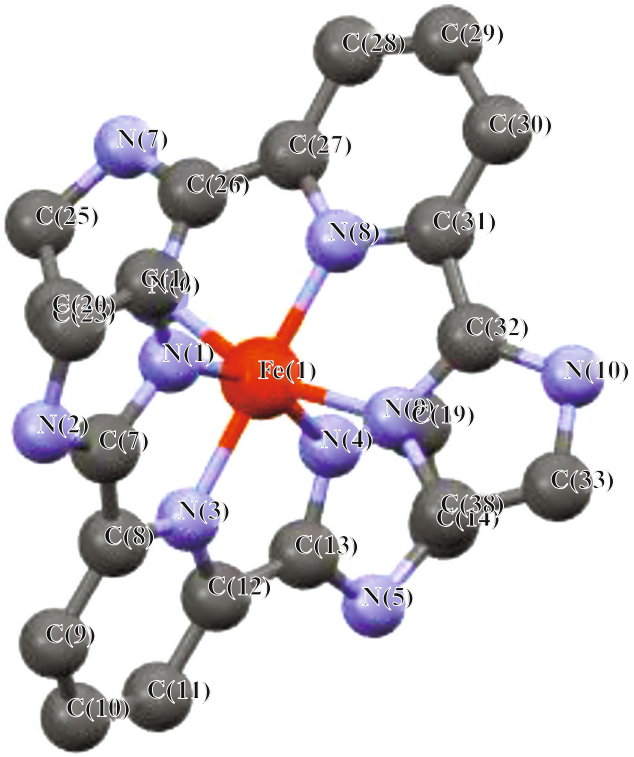

Fig. 5. Structure of the coordination core determined from simulation of the EXAFS spectrum of the $[FeL_2][B_{12}H_{12}] \cdot H_2O$ complex.

the Fourier transform magnitudes of experimental Fe*K* EXAFS spectra ($k^2\chi(k)$) of complexes **1** and **2** not corrected. As follows from Fig. 3, the FT magnitudes for complexes **1** and **2** coincide within the margins of measurement error. This indicates that the structural parameters of the nearest environment of iron(II) ions are similar; therefore, the same model was used to simulate the EXAFS spectra for these two compounds. Heating $[FeL_2][B_{10}H_{10}] \cdot 2H_2O$ to 450 K (high-spin state) does not lead to radical changes in the structure of the environment of the iron atom (Fig. 4), no shifts of the maxima are observed, indicating no changes in the corresponding interatomic distances. One can only note a decrease in the amplitude of the maxima due to an increase in the temperature part of

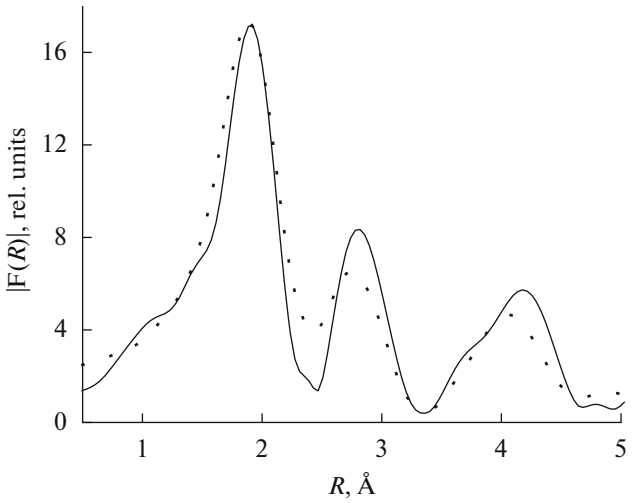

Fig. 6. Fourier transform magnitudes of (solid line) experimental and (dashed line) simulated Fe*K* EXAFS spectra ($k^2\chi(k)$) of the $[FeL_2][B_{12}H_{12}] \cdot H_2O$ complex. Measurements were performed at room temperature.

the Debye factor. Figure 5 and Table 4 show the structural data for the coordination core obtained in the course of simulation of the EXAFS spectrum of the $[FeL_2][B_{12}H_{12}] \cdot H_2O$ complex. The accuracy of determination of interatomic distances from EXAFS data is ±1% (for the nearest sphere of the environment). Figure 6 shows the Fourier transform magnitudes of the experimental (solid line) and simulated (dashed line) Fe*K* EXAFS spectra ($k^2\chi(k)$) of the $[FeL_2][B_{12}H_{12}] \cdot H_2O$ complex. Measurements were performed at room temperature.

The results of studying the static magnetic susceptibility of the compounds under study are shown in Figs. 7 and 8. The complexes studied in the empirically selected temperature ranges of their stability demonstrate spin crossover both in the presence of water of crystallization and in the dehydrated state. The temperatures of the direct and reverse transitions are presented in Table 5.

In the high-spin state of the crystal water-containing complexes, $\mu_{eff} = 4.5–4.7\ \mu_B$ are achieved, which is somewhat lower than the theoretical value of 4.9 μ_B. In the low-spin form of these compounds, residual $\mu_{eff} =$

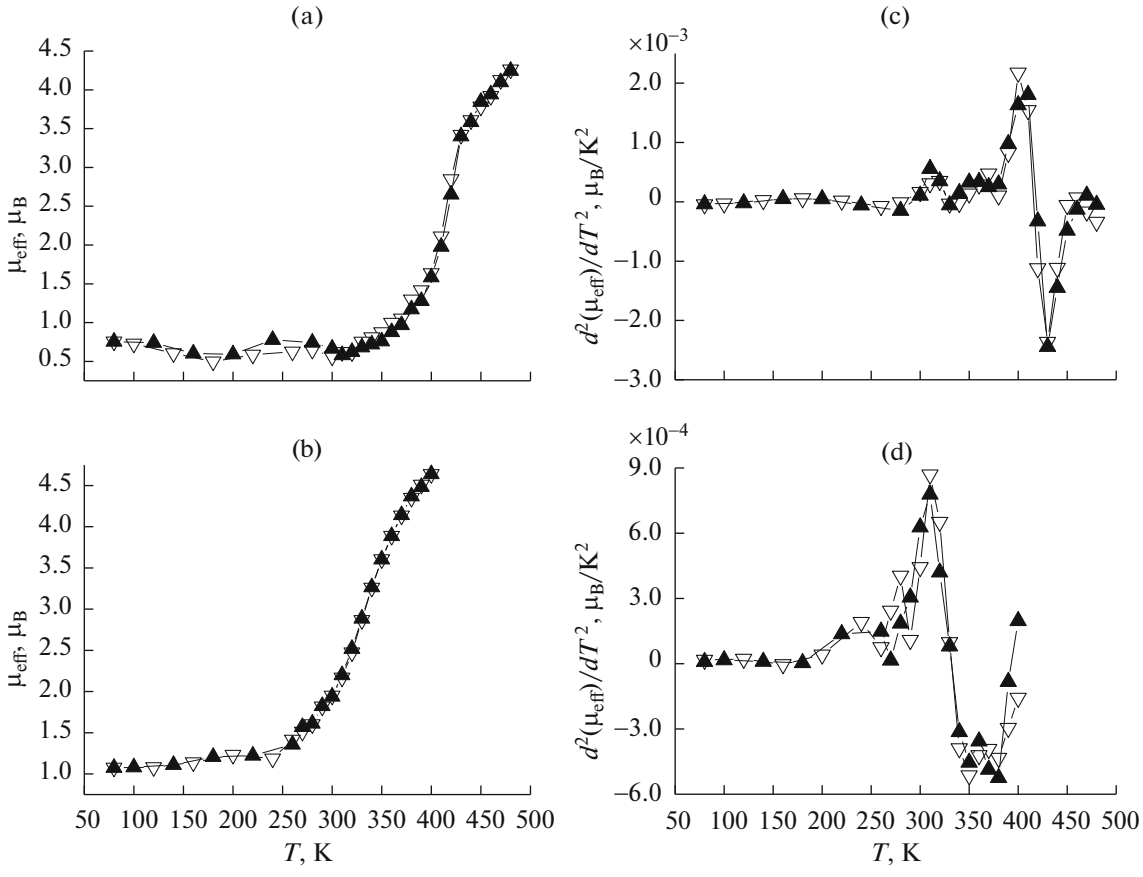

Fig. 7. Temperature dependences of (a and b) μ_{eff} and (c and d) $d^2\mu_{eff}/dT^2$ for $[FeL_2][B_{10}H_{10}] \cdot 2H_2O$ and $[FeL_2][B_{12}H_{12}] \cdot H_2O$, respectively.

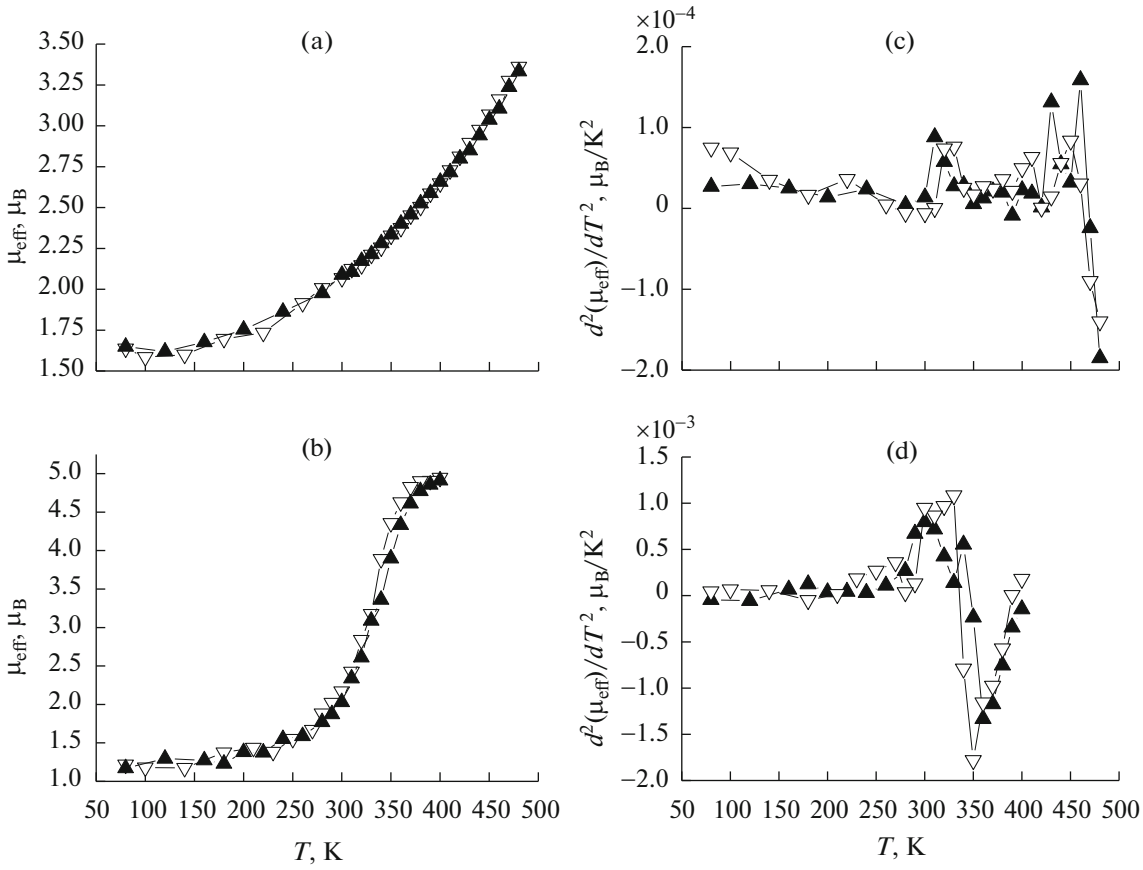

Fig. 8. Temperature dependences of (a and b) μ_{eff} and (c and d) $d^2\mu_{eff}/dT^2$ for the dehydrated complexes $[FeL_2][B_{10}H_{10}]$ and $[FeL_2][B_{12}H_{12}]$, respectively.

0.5–1.0 μ_B are observed. Going from $[FeL_2][B_{10}H_{10}] \cdot 2H_2O$ to $[FeL_2][B_{12}H_{12}] \cdot H_2O$ is accompanied by a decrease in crossover temperatures by ~ 80 K and the disappearance of hysteresis loop (ΔT_c) between the direct and reverse transitions.

Upon dehydration of the complexes, an increase is observed in the maximum transition temperature and the residual magnetic moment in the low-spin state to μ_{eff} = 1.2–1.6 μ_B. The tendency towards a decrease in the SCO temperature remains on going from $[FeL_2][B_{10}H_{10}]$ to $[FeL_2][B_{12}H_{12}]$. For $[FeL_2][B_{10}H_{10}]$ in the temperature range of stability, μ_{eff} = 3.3 μ_B is achieved. With the removal of water molecules of crystallization, an increase/appearance of hysteresis between the direct and reverse transitions is also observed (Table 5).

Table 4. Selected bond lengths and bond angles in the structure of the $[FeL_2][B_{12}H_{12}] \cdot H_2O$ complex according to EXAFS data

Bond	d, Å	Angle	ω, deg
Fe(1)–N(8)	1.90	N(1)Fe(1)N(8)	102.9
Fe(1)–N(1)	1.95	N(1)Fe(1)N(6)	93.3
Fe(1)–N(9)	1.98	N(1)Fe(1)N(9)	93.6
Debye–Waller factor σ^2(Fe–N), Å^2	0.009; T = 300 K 0.014; T = 450 K		
F_{EXAFS}[a]	1.6		

[a] $F_{EXAFS} = \sum_i^N w_i^2 \left(\chi_i^{exp}(k) - \chi_i^{th}(k)\right)^2$, $w_i = \dfrac{k_i^n}{\sum_i^N k_i^n \left|\chi_j^{exp}(k)\right|}$.

F_{EXAFS} is the fitting factor characterizing simulation quality. The accuracy of determination of interatomic distances from EXAFS data is ±1% (for the nearest sphere of the environment) and that of partial coordination numbers, ±10–20%.

Table 5. Temperatures of the direct ($T_c\uparrow$) and reverse ($T_c\downarrow$) transitions for the $[FeL_2]A \cdot nH_2O$ complexes

Compound	$T_c\uparrow$, K	$T_c\downarrow$, K	ΔT_c, K
$[FeL_2][B_{10}H_{10}] \cdot 2H_2O$	419	416	3
$[FeL_2][B_{12}H_{12}] \cdot H_2O$	332	332	0
$[FeL_2][B_{10}H_{10}]$	468	463	5
$[FeL_2][B_{12}H_{12}]$	347	336	11

The results of the study of the obtained complexes and comparison with the literature [16, 17] and our earlier data [18, 19] show that the $[FeL_2][B_{10}H_{10}] \cdot 2H_2O$ and $[FeL_2][B_{12}H_{12}] \cdot H_2O$ complexes have an octahedral coordination polyhedron. Two ligands are coordinated to the iron(II) ion in a tridentate cyclic mode through two nitrogen atoms of the imidazole rings and the pyridine nitrogen atom to form the FeN_6 coordination core.

CONCLUSIONS

New iron(II) *closo*-borate complexes with 2,6-bis(benzimidazole-2-yl)pyridine $[FeL_2][B_{10}H_{10}] \cdot 2H_2O$ and $[FeL_2][B_{12}H_{12}] \cdot H_2O$ have been synthesized. It has been demonstrated that both the initial compounds and their dehydrated analogues exhibit thermo-induced spin crossover ${}^1A_1 \Leftrightarrow {}^5T_2$. The SCO temperatures significantly depend on the composition of the outer-sphere anion: the T_c values of $[FeL_2][B_{10}H_{10}] \cdot 2H_2O$ and $[FeL_2][B_{10}H_{10}]$ are significantly higher than T_c for $[FeL_2][B_{12}H_{12}] \cdot H_2O$ and $[FeL_2][B_{12}H_{12}]$.

ACKNOWLEDGMENTS

We are grateful to N.P. Korotkevich for recording the X-ray powder diffraction patterns and to I.V. Yushina for recording the diffuse reflectance spectra.

FUNDING

The work was partially supported by the Russian Science Foundation (project no. 20-63-46026).

CONFLICT OF INTEREST

The authors declare no conflict of interest.

REFERENCES

1. *Spin Crossover in Transition Metal Compounds I–III*, Ed. by P. Gütlich and H. Goodwin (Springer, 2004).
2. M. A. Halcrow, *Spin-Crossover Materials Properties and Applications* (Wiley, 2013).
3. O. Kahn, J. Kröber, and C. Jay, Adv. Mater. **4**, 718 (1992).
4. L. G. Lavrenova and O. G. Shakirova, Eur. J. Inorg. Chem, 670 (2013).
5. M. Shatruk, H. Phan, B. A. Chrisostomo, and A. Suleimenova, Coord. Chem. Rev. **289–290**, 62 (2015).
6. H. L. C. Feltham, A. S. Barltrop, and S. Brooker, Coord. Chem. Rev. **344**, 26 (2017).
7. H. S. Scott, R. W. Staniland, and P. E. Kruger, Coord. Chem. Rev. **362**, 24 (2018).
8. O. G. Shakirova, L. G. Lavrenova, A. S. Bogomyakov, et al., Russ. J. Inorg. Chem. **60**, 786 (2015).
9. E. N. Frolova, T. A. Ivanova, O. A. Turanova, et al. Russ. J. Inorg. Chem. **63**, 1012 (2018).
10. P. Gamez, J. S. Costa, M. Quesada, and G. Aromí, Dalton Trans., 7845 (2009).
11. S. Hayami, S. M. Holmes, and M. A. Halcrow, J. Mater. Chem. C **3**, 7775 (2015).
12. M. Matsuda, H. Isozaki, and H. Tajima, Chem. Lett. **37**, 374 (2008).
13. R. N. Muller, V. Elst, and S. Laurent, J. Am. Chem. Soc. **125**, 8405 (2003).
14. J.-F. Letard, N. Daro, C. Aymonier, et al., Patent EP2391631 (2011).
15. A. Bousseksou, C. Vieu, J.-F. Letard, et al., EU Patent 1430552 (2004).
16. M. Boča, R. F. Jameson, and W. Linert, Coord. Chem. Rev. **255**, 290 (2011).
17. R. Boča, P. Baran, M. Boča, et al., Inorg. Chim. Acta **278**, 190 (1998).
18. L. G. Lavrenova, I. I. Dyukova, E. V. Korotaev, et al., Russ. J. Inorg. Chem. **65**, 30 (2020).
19. A. D. Ivanova, E. V. Korotaev, V. Yu. Komarov, et al., New J. Chem. **44**, 5834 (2020).
20. I. B. Sivaev, V. I. Bregadze, and N. T. Kuznetsov, Izv. Akad. Nauk, Ser. Khim., No. 8, 1256 (2002).
21. M. F. Hawthorne, Mol. Med. Today **4**, 174 (1998).
22. Y. Zhu, Y. Lin, Y. Z. Zhu, et al., J. Nanomater. **2010**, art. 409320 (2010).
23. V. V. Avdeeva, E. A. Malinina, and N. T. Kuznetsov, Russ. J. Inorg. Chem. **62**, 1673 (2017).
24. S. E. Korolenko, V. V. Avdeeva, E. A. Malinina, et al., Russ. J. Coord. Chem. **46**, 297 (2020).
25. O. G. Shakirova, L. G. Lavrenova, and V. N. Ikorskiy, et al., Chem. Sust. Dev. **10**, 757 (2002).
26. M. B. Bushuev, L. G. Lavrenova, Yu. G. Shvedenkov, et al., Russ. J. Coord. Chem. **34**, 190 (2008).
27. O. G. Shakirova, V. A. Daletskii, L. G. Lavrenova, et al., Russ. J. Inorg. Chem. **58**, 650 (2013).
28. H. C. Miller and E. L. Muetterties, Inorg. Synth. **10**, 81 (1967).
29. A. Lever, *Inorganic Electronic Spectroscopy* (Elsevier, Amsterdam, 1984; Mir, Moscow, 1987).
30. A. Hauser, Top Curr. Chem. **233**, 49 (2004).
31. S. Sugano, Y. Tanabe, and H. Kamimura, *Multiplets of Transition-Metal Ions in Crystals* (Academic Press Pure and Applied Physics, New York, 1970).

Translated by G. Kirakosyan